Oxygen Release and Exchange in Niobium Oxide MEHPPV Hybrid Solar Cells

Monica Lira-Cantu,† Kion Norrman, Jens W. Andreasen, and Frederik C. Krebs*

The Danish Polymer Centre, Risø National Laboratory, P.O. Box 49, DK-4000 Roskilde, Denmark

Received June 20, 2006. Revised Manuscript Received August 16, 2006

We demonstrate that niobium oxide exchanges oxygen with the atmosphere when illuminated by simulated sunlight. The oxygen exchange was found to take place for pristine niobium oxide films when illuminated in an oxygen atmosphere and when illuminated in an operational hybrid solar cell. The oxygen exchange was demonstrated using $^{18}O_2$-isotopic labeling in combination with time-of-flight secondary ion mass spectrometry (TOF-SIMS) imaging analysis of devices and oxide substrates. TOF-SIMS depth profiling confirmed ^{18}O incorporation throughout the device in hybrid solar cells. The results are discussed in the context of hybrid solar cell stability and illuminate one of the degradation paths.

Introduction

Hybrid solar cells (HSC) are typically composed of an electron transporting inorganic semiconductor material and a conjugated organic polymer material.[1−6] When the electron transporting material is an inorganic oxide, these solar cells operate and produce a current in an external circuit by exciton dissociation at the oxide−polymer interface that leads to electron injection and transport through the oxide and hole transport through the polymer. Electron transport and charge-transfer processes in polymer-organic solar cells are believed to be the biggest hindrance for obtaining high efficiency devices and the current state-of-the-art employ a nanostructured morphology in the form of a bulk heterojunction.[7] The bulk heterojunction has been realized as a mixture of a conjugated polymer (e.g., P3HT, MEHPPV, MDMOPPV) and a fullerene derivative[8] (i.e., PCBM) or as a mixture of the conjugated polymer and semiconductor nanoparticles, nanorods, or well-ordered nanostructures (e.g., TiO_2, ZnO, or CdSe).[9−25] One advantage of the HSCs employing a conjugated polymer and nanostructured materials is a superior morphological stability. In the case of bulk heterojunctions based on P3HT and PCBM it has been shown that the appropriate morphology required for high efficiency is obtained only through elaborate and careful processing during film formation and by thermal annealing at temperatures around 100 °C.[26] The pioneering work by Arango and Carter[27] and more recently by Beek et al.[10,28,29] has demonstrated that promising and highly efficient HSCs incorporating semiconductor oxides can be fabricated. Despite these discoveries, generating solar cells with long lifetimes[30,31] is a great challenge, and the elucidation of possible degradation mechanisms could pave the way for stable HSC devices. We

† Present address: Institut de Ciència de Materials de Barcelona (CSIC), Campus UAB, E-08193 Bellaterra, Spain.

(1) Brabec, C. J.; Sariciftci, N. S.; Hummelen, J. C. *Adv. Funct. Mater.* **2001**, *11*, 15−26.
(2) Spanggaard, H.; Krebs, F. C. *Sol. Energy Mater. Sol. Cells* **2004**, *83*, 125−146.
(3) Coakly, K. M.; McGehee, M. D. *Chem. Mater.* **2004**, *16*, 4533−4542.
(4) Hoppe, H.; Sariciftci, N. S. *J. Mater. Res.* **2004**, *19*, 1924−1945.
(5) Special Issue: The Development of Organic and Polymer Photovoltaics. *Sol. Energy Mater. Sol. Cells* **2004**, *83*, issues 2−3.
(6) Special Issue: Organic-Based Photovoltaics. *MRS Bull.* **2005**, *30*, issue 1.
(7) (a) Yu, G.; Gao, J.; Hummelen, J. C.; Wudl, F.; Heeger, A. J. *Science* **1995**, *270*, 1789−1791. (b) Forrest, S. R. *Mater. Res. Soc. Bull.* **2005**, *30*, 28−32.
(8) Geens, W.; Martens, T.; Poortmans, J.; Aernouts, T.; Manca, J.; Lutsen, L.; Heremans, P.; Borghs, S.; Mertens, R.; Vanderzande, D. *Thin Solid Films* **2004**, *451−452*, 498−502.
(9) Arango, A. C.; Johnson, L. R.; Bliznyuk, V. N.; Schlesinger, Z.; Carter, S. A.; Hörhold, H.-H. *Adv. Mater.* **2000**, *12*, 1689−1692.
(10) Beek, W. J. E.; Wienk, M. M.; Janssen, R. A. J. *Adv. Mater.* **2004**, *16*, 1009−1013.
(11) Coakley, K. M.; Liu, Y.; Goh, C.; McGehee, D. M. *Mater. Res. Soc. Bull.* **2005**, *30*, 37−40.
(12) Milliron, D. J.; Gur, I.; Alivisatos, A. P. *Mater. Res. Soc. Bull.* **2005**, *30*, 41−44.
(13) Alivisatos, A. P. *Science* **1996**, *271*, 933.
(14) Sloof, L. H.; Wienk, M. M.; Kroon, J. M. *Thin Solid Films* **2004**, *451−452*, 634−638.
(15) Sloof, H.; Kroon, J. M.; Loos, J.; Koetse, M. M.; Sweelssen, J. *Adv. Funct. Mater.* **2005**, *15*, 689−694.
(16) Ravirajan, P.; Haque, S. A.; Poplavskyy, D.; Durrant, J. R.; Bradley, D. D. C.; Nelson, J. *Thin Solid Films* **2004**, *451−452*, 624−629.
(17) Kwong, C. Y.; Choy, W. C. H.; Djurisic, A. B.; Chui, P. C.; Cheng, K. W.; Chan, W. K. *Nanotechnol.* **2004**, *15*, 1156−1161.
(18) Wallace, G. G.; Dastoor, P. C.; Officer, D. L.; Too, C. O. *Photon* **2000**, *30*, 14−22.
(19) Coakley, K. M.; Liu, Y. X.; McGehee, M. D. *Abstracts of Papers of the American Chemical Society* **2004**, *227*, U424−U424.
(20) Coakley, K. M; Liu, Y. X.; McGehee, M. D.; Frindell, K. L.; Stucky, G. D. *Adv. Funct. Mater.* **2003**, *13*, 301−306.
(21) Greenham, N. C.; Peng, X.; Alivisatos, A. P. *Phys. Rev. B* **1996**, *54*, 17628.
(22) Huynh, W. U.; Dittmer, J. J.; Teclemariam, N.; Milliro, D. J.; Alivisatos, A. P.; Barnham, K. W. J. *Phys. Rev. B* **2003**, *67*, 115326.
(23) Huynh, W. U.; Dittmer, J. J.; Libby, W. C.; Whitting, G. L.; Alivisatos, A. P. *Adv. Funct. Mater.* **2003**, *13*, 73.
(24) Grätzel, M. *Mater. Res. Bull* **2005**, *30*, 23−28.
(25) Breeze, A. J.; Schlesinger, Z.; Carter, S. A.; Brock, P. J. *Phys. Rev. B* **2001**, *64*, 125205.
(26) Li, G.; Shrotriya, V.; Huang, J.; Yao, Y.; Moriarty, T.; Emery, K.; Yang, Y. *Nat. Mater.* **2005**, *4*, 864−868.
(27) Arango, A. C.; Carter, S. A. *Appl. Phys. Lett.* **1999**, *74*, 1698−1700.
(28) Beek, W. J. E.; Wienk, M. M.; Janssen, R. A. J. *J. Mater. Chem.* **2005**, *15*, 2985−2988.
(29) Beek, W. J. E.; Wienk, M. M.; Kemerink, M.; Yang, M.; Janssen, R. A. J. *J. Phys. Chem. B* **2005**, *109*, 9505−9516.
(30) Yang, X.; Loos, J.; Veenstra, S. C.; Verhees, W. J. H.; Wienk, M. M.; Kroon, J. M.; Michels, M. A. J.; Janssen, R. A. J. *Nano Lett.* **2005**, *5*, 579−583.
(31) Krebs, F. C.; Spanggaard, H. *Chem. Mater.* **2005**, *17*, 5235−5237.

10.1021/cm061429d CCC: $33.50
Published on Web 10/25/2006

have studied HSCs based on different thin film semiconductor oxides, ZnO, TiO_2, CeO_2, Nb_2O_5, and CeO_2-TiO_2 with special focus on the operational stability in air,[32−35] and have documented a delicate interplay between atmospheric oxygen and operation of the photovoltaic device. In an effort to understand HSC degradation we analyzed the effect of different atmospheres on HSC performance and lifetime and found that photovoltaic properties are improved when devices are analyzed in an oxygen-containing atmosphere. The photovoltaic properties were studied by recording the IV-curves by sourcing a voltage and measuring the current passing through the device under illumination and in the dark. Under illumination the intercept with the voltage axis gives the open circuit voltage (V_{oc}) which is equivalent to the maximum voltage the device can produce. The intercept with the current axis gives the short circuit current (I_{sc}) which is equivalent to the maximum current the device can produce. The maximum power that can be extracted from the device during photovoltaic operation is smaller than the product of V_{oc} and I_{sc} by a factor known as the fill factor (FF). The changes in these parameters were used as a measure of the change in the device performance. The aim of this study was to investigate the interaction between the constituents of the device and oxygen during operation. The HSC configuration applied in this work is glass/indium tin oxide (ITO)/$Nb_2O_{5thin\ film}$/MEHPPV/Ag. Analyses of V_{oc}, I_{sc}, IV-curves, and photophysical properties under inert and ambient atmosphere were carried out. We also analyzed the stability of the HSC by blocking the UV wavelength range (<400 nm) by applying a UV filter. Our results show that atmospheric oxygen is incorporated in the semiconductor oxide during illumination and that it improves the performance of the HSC. Our results have been supported by further testing the HSC under an $^{18}O_2$ atmosphere with subsequent characterization using time-of-flight secondary ion mass spectrometry (TOF-SIMS) imaging, X-ray reflectometry, and TOF-SIMS depth profiling.

Experimental Section

Materials. The synthesis of MEHPPV was carried out according to the literature.[36] Niobium(V) ethoxide was purchased at Aldrich and used as received. Acetylacetone was purchased from Merck, and 65% nitric acid was purchased from Riedel-de Haën. All materials were used without further purification. Chlorobenzene was purchased from Aldrich (99.5%). Zinc acetate, diethanol amine, and isopropanol were purchased from Aldrich and used as received. ITO substrates were purchased from Delta Technologies, Ltd. (USA). The substrate dimensions were 25 × 50 × 1.1 mm (coated on one surface, Rs = 10 Ω ± 5 Ω) and were etched and prepared following a method described earlier.[37] Once etched the substrates were washed with acetone and ethanol in an ultrasonic bath for 10 min, respectively.

Nb_2O_5 Thin Film Preparation. For the preparation of the Nb_2O_5 thin films a modification of a method described in the literature[38] was applied. A total of 4.5 mL of niobium(V) ethoxide (99.95%) was mixed with 3 mL of ethanol (99.9%) and 0.015 mL (approximately 2 drops) of acetic acid, after which the mixture was stirred for 15 min. After the preparation of this concentrated solution, 0.5 mL was mixed with 10 mL of ethanol (99.9%). Ethanol was carefully added drop by drop, up to a volume of 10 mL (some turbidity was observed but disappeared after 2 h of stirring). The final precursor solution was filtered with a 0.45 μm filter. The solution is stable for a maximum of 2 weeks and presents turbidity and a white precipitate after a couple of days. The Nb_2O_5 thin films were prepared by spin coating the as-prepared solution on ITO substrates between 1500 and 3000 rpm for 30 s. The film was calcined at 450 °C for 2 h controlling the heating rate at 3 °C min^{-1}. Once sintered the thin Nb_2O_5 surface was transparent and presented a light purple-blue color.

Polymer Photovoltaic Preparation. Photovoltaic devices were prepared by spin coating a microfiltered MEHPPV polymer solution (0.45 μm) from chlorobenzene at 1500 rpm for 30 s on top of the glass/ITO/semiconducting oxide substrates. The glass/ITO/thin film semiconductor oxide substrate was heated to 100 °C for 10 min prior to use to dry the surface. The substrates were then cleaned with chloroform (via spin coating) before the polymer solution was applied. The absorbance of the spin-coated polymer films was controlled to be between 0.9−1 absorbance units unless otherwise specified. The active area of the devices were 3.3 ± 0.2 cm^2. Silver electrodes were thermally evaporated onto the polymer film at a pressure of $<10^{-5}$ mbar through a shadow mask. The device was mounted using conductive silver epoxy glue for the electrical contacts. In cases where devices were tested under vacuum the pressure was maintained below 10^{-5} mbar. The influence of the atmosphere was established by illumination in the ambient atmosphere or in a vacuum chamber with a quartz window.[39]

Polymer Photovoltaic Characterization. The electrical measurements were carried out using a Keithley 2400 Sourcemeter. The positive terminal of the Keithley Sourcemeter was attached to the glass/ITO/oxide, and the negative terminal was attached to the metal electrode. This deliberate choice was made in order to distinguish the function of the transparent conducting oxide (TCO) and metal electrode as compared to traditional polymer photovoltaics where the TCO is the hole collector and the metal is the electron collector. The wavelength dependence of the photovoltaic response was characterized using a setup described elsewhere,[39] and the photovoltaic response under simulated sunlight was determined using calibrated sun simulators (KHS Solar Konstant 575 from Steuernagel Lichttechnik GmbH, Germany). The spectral distribution and quality of the solar simulator was monitored using a spectrometer from AvaSpec 2048 from Avantes. The spectral distribution was AM 1.5, and the simulator is class A in the wavelength range 400−700 nm according to the ASTM E927 standard. A precision Pyranometer from Eppley Laboratories was used to monitor the total power that was set to 1000 W m^{-2} in all experiments. Details of the performance, spectral match, and so forth can be found at our website (http://www.risoe.dk/solarcells/pdf/KHS_routine_test.pdf). The action spectra dependence of the photovoltaic response was characterized using a setup described in the literature with cylindrical lenses in order to narrow the spectral

(32) Lira-Cantu, M.; Krebs, F. C. *Sol. Energy Mater. Sol. Cells* **2006**, *90*, 2076−2086.
(33) Lira-Cantu, M.; Krebs, F. C. *Recent Res. Dev. Appl. Phys.* **2005**, *8*, 71−98.
(34) Lira-Cantu, M.; Krebs, F. C. U.K. Patent GB05097667.0, May 15, 2005.
(35) Lira-Cantu, M.; Krebs, F. C. U.K. Patent GB0607669.9, April 25, 2006.
(36) Neef, C. J.; Ferraris, J. P. *Macromolecules* **2000**, *33*, 2311−2314.
(37) Krebs, F. C.; Carlé, J. E.; Cruys-Bagger, N.; Andersen, M.; Lilliedal, M. R.; Hammond, M. A.; Hvidt, S. *Sol. Energy Mater. Sol. Cells* **2005**, *86*, 499−516.
(38) Özer, N.; Chen, D.-G.; Lampert, C. M. *Thin Solid Films* **1996**, *277*, 162−168.
(39) Krebs, F. C.; Jørgensen, M. *Rev. Sci. Instrum.* **2003**, *74*, 3438−3441.

bandwidth to 10 nm.[39] The polymer film thicknesses were determined by atomic force microscopy.

$^{18}O_2$ Labeling. Two HSCs with a glass/ITO/Nb_2O_5/MEHPPV/Ag geometry were introduced into a modified Schlenk tube (Trallero) with a 250 mL volume. One of the devices was illuminated at 1000 W m^{-2}, and the other was kept in the dark under the same atmosphere and used as the reference. After a few minutes in air the tube with the two samples was purged with argon. The I_{sc} of the sample was monitored until the current density had decreased by more than 50% of the initial value. The argon flux was then stopped and $^{18}O_2$ gas was introduced. Changes in I_{sc} were monitored continuously until the I_{sc} stabilized for 30 min. Irradiation was then stopped and the samples were stored in darkness during transfer to the TOF-SIMS instrument. Before TOF-SIMS analysis a part of the silver electrode was peeled off by attaching 3M adhesive tape to the silver electrode followed by removal. The tape neatly adhered to the silver and separated it from the active layer. Pristine Nb_2O_5 substrates were exposed to $^{18}O_2$ under the same conditions but for 48 h instead.

Characterization by TOF-SIMS. The TOF-SIMS imaging analyses were performed using a TOF-SIMS IV (Ion-Tof GmbH, Münster, Germany) operated at a pressure of 5×10^{-8} mbar (with sample). Twenty-five nanosecond pulses of 25 keV Bi_3^+ (primary ions) were bunched to form ion packets with a nominal temporal extent of <1 ns at a repetition rate of 5 kHz thus yielding a target current of 50 fA. Images were acquired over a 25×10 mm^2 area of the device. TOF-SIMS depth profiling was achieved using the same conditions for the analysis gun and the following conditions for the sputter gun: 3 keV Xe^+ (sputter ions) was used at a target current of 7 nA. A 400×400 μm^2 area of the sample was sputtered, and the central 50×50 μm^2 area was analyzed. Desorbed secondary ions were accelerated to 2 keV, mass analyzed in the flight tube, and post-accelerated to 10 keV before detection.

Characterization by X-ray Reflectometry. We have measured the reflectivity profile of a HSC, consisting of ITO coated glass, covered by a layer of niobium oxide (nominally Nb_2O_5). The polymer layer was removed before the reflectivity measurement. The data were acquired at the "Butterfly 2" instrument at the Nanoscience centre at University of Copenhagen. The instrument is equipped with a Seifert sealed X-ray Cu tube operating at 40 kV, 20 mA. The emitted Cu Kα X-rays are focused by multilayer optics (Osmic) and collimated with slits. The reflected intensity was recorded with a Cyberstar scintillation point detector. Measurement of the reflectivity profile up to scattering vector $q = 0.45$ $Å^{-1}$ was completed in 100 min. The X-ray reflectivity was calculated for models of the scattering length density (SLD) distribution, using the dynamical formalism of Parratt.[40] The density profiles were represented by 250-bin histograms. The density profile was fitted by minimizing a goodness-of-fit figure evaluated as a weighted sum of normalized residuals and a function penalizing SLD profile length, the latter preventing the solutions from displaying unphysical oscillations. The SLD of each bin was constrained to vary within a few percent of the calculated theoretical values, assuming mass densities of 2.2 g cm^{-3} for SiO_2 glass, 4.47 g cm^{-3} for Nb_2O_5, and 7.14 g cm^{-3} for ITO [91 (In_2O_3):9 (SnO_2)]. In addition to the density profile, the effective footprint was fitted to the data. The fitted reflectivity profile is shown in Figure 1a with the inset detailing a part of the curve clearly showing the short period Kiessig fringes representing the thick ITO layer, decorating the longer period fringes of the thinner Nb_2O_5 layer. The fitted SLD profile is shown as Figure 1b. From the density profile we derive an ITO layer thickness of 87 ± 5 nm (100 nm reported by the supplier) and an Nb_2O_5 thickness of 12 ± 2 nm. The layer interfaces are quite broad relative to the layer thicknesses, but it is not possible by X-ray reflectometry to determine whether this is due to thickness inhomogeneities or interlayer diffusion (graded interfaces).

(40) Parratt, L. G. *Phys. Rev.* **1954**, *95*, 359−369.

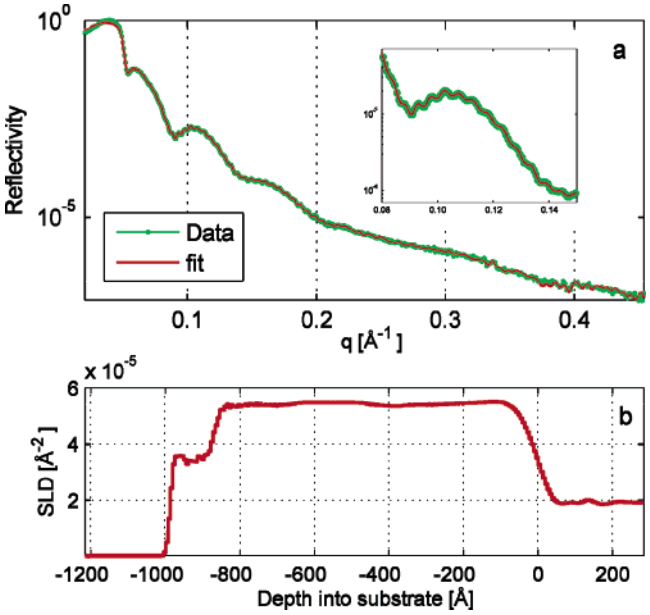

Figure 1. (a) Reflectivity profile of the HSC, data, and fit. The inset shows a detail of the profile, highlighting the short period fringes from the ITO layer. (b) The fitted SLD profile. The substrate is to the right (positive values above zero), and air is to the far left.

Results and Discussion

General Characterization. The photovoltaic properties of the freshly prepared ITO/Nb_2O_5/MEHPPV/Ag large area devices (3.3 cm^2 active area) were found to improve when stored in the ambient atmosphere in the dark for 48 h. The V_{oc}, I_{sc}, and FF typically changed from initial values of −0.04 V and 0.03 mA cm^{-2} (measured immediately after electrode evaporation) up to −0.76 V, 0.28 mA cm^{-2}, and 44% FF after 48 h. The 48 h period in the dark was found to be the best for obtaining optimal photovoltaic properties.

Effect of UV Light and Testing Atmosphere. We have recently reported the lifetime performance, under ambient atmosphere, of HSCs applying different semiconductor oxides and observed polymer bleaching and device degradation at the end of the lifetime.[32] The degradation of the MEHPPV polymer is not surprising if we consider that UV light is known to excite semiconductor oxides generating active oxygen species. Those oxygen species are known to interact with and degrade the MEHPPV polymer. Thus, in order to improve HSC lifetime, we carried out solar decay analyses with special emphasis on factors known to degrade HSC lifetime. The effect of UV light or the testing atmosphere was reported by Beek et al.[28,29] for ZnO nanoparticle−polymer bulk heterojunctions where the application of a UV filter was found necessary during device characterization. The effect of UV light was thus studied by the application of a UV filter that removes wavelengths below 400 nm. Our results confirmed the earlier finding by Beek et al.[28] that the device was more stable when the UV light was blocked by a filter. Without the UV filter the

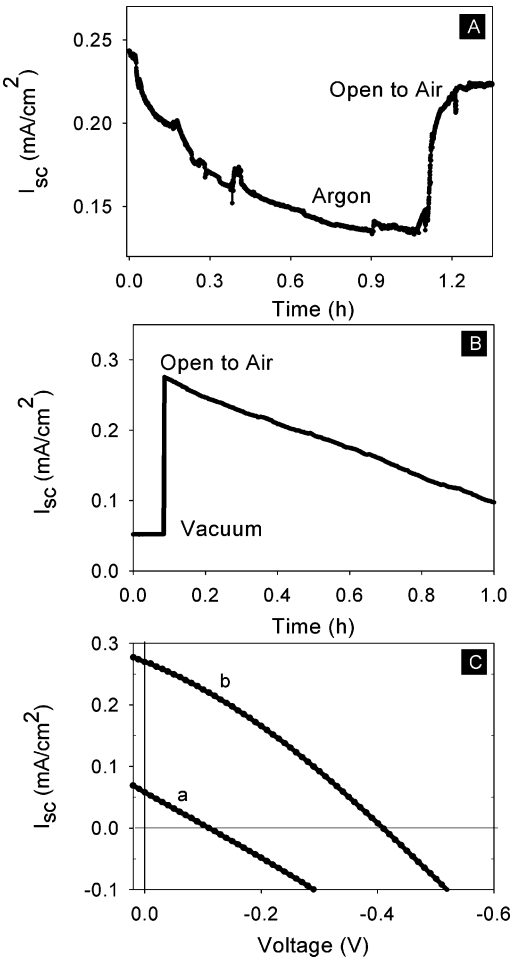

Figure 2. Effect of the atmosphere on a glass/ITO/Nb_2O_5/MEHPPV/Ag device. (A) argon atmosphere, (B) vacuum (1×10^{-6} mbar) with introduction of air, and (C) IV-curves corresponding to the graph in B obtained under vacuum (a) and right after atmospheric oxygen was introduced (b). The atmosphere in graph A was composed of 20% $^{18}O_2$ and 80% N_2. TOF-SIMS analysis was subsequently performed on this device.

devices quickly degraded. Another important factor that can contribute to HSC degradation is oxygen from the atmosphere that is known to photobleach (oxidize) MEHPPV. Thus, working under inert atmospheres or in vacuum could, in principle, suppress the photobleaching and increase the lifetime of the solar cell. In our experiment a HSC was subjected to inert atmospheres and the evolution of the I_{sc} was recorded (Figure 2).

Contrary to or expectations, I_{sc} decreased with time under inert atmospheres (argon or vacuum) as shown in Figure 2A and 2B. The main difference between vacuum and argon was a slower decrease in I_{sc} observed in argon (Figure 2A). In vacuum (Figure 2B) I_{sc} decreases drastically in just a couple of minutes. The low I_{sc} value observed under inert atmosphere was observed for a long time until the sample was taken out of the inert atmosphere chamber and into the ambient atmosphere. Once in the ambient atmosphere, a fast increase in I_{sc} was observed as shown in Figure 2A,B. In addition the performance observed by recording the IV-curves improved immediately when introducing oxygen after having exposed the device to vacuum conditions as shown in Figure 2C. To summarize the facts known from the literature and the results from above we found that the device performance improved upon resting in the ambient atmosphere for 48 h prior to characterization, we confirmed that the lifetime can be improved by the application of a UV filter under ambient conditions and found that no improvement in the performance could be achieved by the elimination of oxygen under inert atmospheres. We attributed the behavior observed in Figure 2 to the semiconductor oxide itself.

Atmosphere−Oxide Interactions. The ambient environment is known to affect the semiconductor oxide properties as reported in the literature.[41−45] Under inert atmosphere transition metal oxides are known to release oxygen[41−49] by formation of O vacancies at the surface. These defects can act as donors of electrons and have a profound influence on the chemical, electrical, and photochemical behavior of transition metal oxides.[41,43,45,47,50] In addition to the latter, some authors have reported the light-driven oxygen scavenging effect of semiconductor oxide/polymer nanocomposites,[51] showing that the presence of oxygen is required for the semiconductor oxide to work as an electron acceptor, especially under irradiation with sunlight.[51] In the absence of oxygen the extraction of O from the semiconductor oxide surface will take place without the possibility of regeneration. The physical, chemical, and electronic properties of the surface thus change with time as observed for our HSC devices (Figure 2). A similar behavior has been observed by Watanabe et al.[52] and van de Zanden et al.[53] who reported that the detrimental effect of inert atmospheres on HSC are due to the formation and stabilization of long-lived trapped charge carriers. Once the HSC is transferred back to the ambient atmosphere, oxygen can be re-adsorbed onto the metal oxide surface[43−45] regenerating the capacity of the semiconductor oxide to act as an electron acceptor,[46,47,51,54,55] thus improving HSC performance. On the basis of these observations we believe that the solar cell response depends upon the equilibrium between oxygen and semiconductor oxides under different atmospheres. We do not ascribe a significant role of UV light as responsible for the degradation of the performance under inert atmospheres. The experiments

(41) Miyaoka, H.; Mizutani, G.; Sano, H.; Omote, M.; Nakatsuji, K.; Komori, F. *Solid State Commun.* **2002**, *123*, 399−404.
(42) Brajsa, A.; Szaniawska, K.; Barczynski, R. J.; Murawski, L.; Kosciel-ska, B.; Vomvas, A.; Pomoni, K. *Opt. Mater.* **2004**, *26*, 151−153.
(43) Tilocca, A; Selloni, A. *Chem. Phys. Chem.* **2005**, *6*, 1911−1916.
(44) Eppler, A. M.; Ballard, I. M.; Nelson, J. *Physica E* **2002**, *14*, 197−202.
(45) Wahlstrom, E.; Vestergaard, E. K.; Schaub, R.; Rønnau, A.; Vester-gaard, M.; Lægsgaard, E.; Stensgaard, I.; Besenbacher, F. *Science* **2004**, *303*, 511−513.
(46) Weidmann, J.; Dittrich, T.; Konstantinova, E.; Lauermann, L.; Uhlendorf, I.; Koch, F. *Sol. Energy Mater. Sol. Cells* **1998**, *56*, 153−165.
(47) Schaub, R.; Wahlström, E.; Rønnau, A.; Laegsgaard, E.; Stensgaard, I.; Besenbacher, F. *Science* **2003**, *299*, 377−379.
(48) Sol, C.; Tilley, J. D. *J. Mater. Chem.* **2001**, *11*, 815−820.
(49) Chaabouni, F.; Abaab, M.; Rezig, B. *Sens. Actuators, B* **2004**, *100*, 200−204.
(50) (a) Yoon, D. K.; Choi, G. M. *Sens. Actuators, B* **1997**, *45*, 251−257. (b) Yu, J. H.; Choi, G. M. *Sens. Actuators, B* **1998**, *52*, 251−256.
(51) Xiao-e, L.; Green, A. N. M.; Haque, S. A.; Mills, A.; Durrant, J. R. *J. Photochem. Photobiol. A* **2004**, *162*, 253−259.
(52) Watanabe, A.; Kasuya, A. *Thin Solid Films* **2005**, *483*, 358−366.
(53) Van der Zanden, B.; Gooses, A. *J. Appl. Phys.* **2003**, *94*, 6959−6965.
(54) Grätzel, M. *Nature* **2001**, *414*, 338−344.
(55) Umeda, T.; Hashimoto, Y.; Mizukami, H.; Shirakawa, T.; Fujii, A.; Yoshino. K. *Appl. Phys. Lett.* **2004**, *85*, 3139−3141.

under inert atmospheres exhibited the same degradation of the response regardless of the presence or absence of a UV filter.

Oxygen in the HSC Devices. From an experimental point of view it is not trivial to elaborate on the interaction between the constituents of the device and oxygen during HSC operation since oxygen is present everywhere and it is difficult to unequivocally demonstrate whether particular oxygen species stem from the experiment under normal test conditions. Oxygen could come from the atmosphere in the form of molecular oxygen or water. Oxygen could also come from MEHPPV since oxygen bridges the conjugated polymer backbone and the alkyl side chain. In order to avoid this ambiguity an atmosphere where the isotope of oxygen ^{16}O is replaced by ^{18}O was employed. In such an experiment it becomes possible to monitor where the oxygen interacts in the device.[56,57] By further employing a mass spectrometric imaging technique such as TOF-SIMS imaging it becomes possible to extract detailed chemical information coupled to the geometry of the device. The TOF-SIMS measurements were furthermore carried out in conjunction with sputtering whereby depth profiling was achieved thus giving full three-dimensional imaging of the ^{18}O distribution in the device.[57]

The experiment was performed by irradiating a solar cell of Nb_2O_5 under argon conditions followed by transfer of the device into a controlled $^{18}O_2$ atmosphere. I_{sc} was monitored during the entire experiment after which the sample was subjected to TOF-SIMS analysis. The results from a TOF-SIMS depth profiling experiment where an $^{18}O_2$ atmosphere was used to establish the path followed by oxygen during testing are shown in Figure 3A. The poor depth resolution could to some extent be the result of interlayer mixing after device fabrication. However, the major contributor is most likely interlayer mixing caused by the sputter process. In spite of the poor depth resolution it is still possible to distinguish the layers, which enable tracking of ^{18}O incorporation in the device. In Figure 3B the $^{18}O/^{16}O$ ratio is plotted against the sputter time together with the depth profile for Nb_2O_5. As is evident from Figure 3B there seems to be ^{18}O incorporation in the Ag, MEHPPV, and the Nb_2O_5 layer. We have previously demonstrated that oxygen penetrates and reacts with the electrode and active (organic) layers of a photovoltaic device.[57] The time window indicated by the two vertical dashed lines (Figure 3B) shows where both ^{18}O incorporation and Nb_2O_5 was detected. However, due to the interlayer mixing and the fact that the MEHPPV layer incorporates atmospheric oxygen (irreversible photo-oxidation), it is not possible to conclude unequivocally that the Nb_2O_5 layer has incorporated ^{18}O from this experiment alone. To elaborate on this the Ag electrode was removed using adhesive tape and the MEHPPV layer was washed off using chloroform on a cotton stick. A part of the exposed device surface was then analyzed using TOF-SIMS imaging. Figure 4A is a schematic of a device that shows which part (dashed red box) was subjected to TOF-SIMS imaging, which includes part of what used to be (before removal of

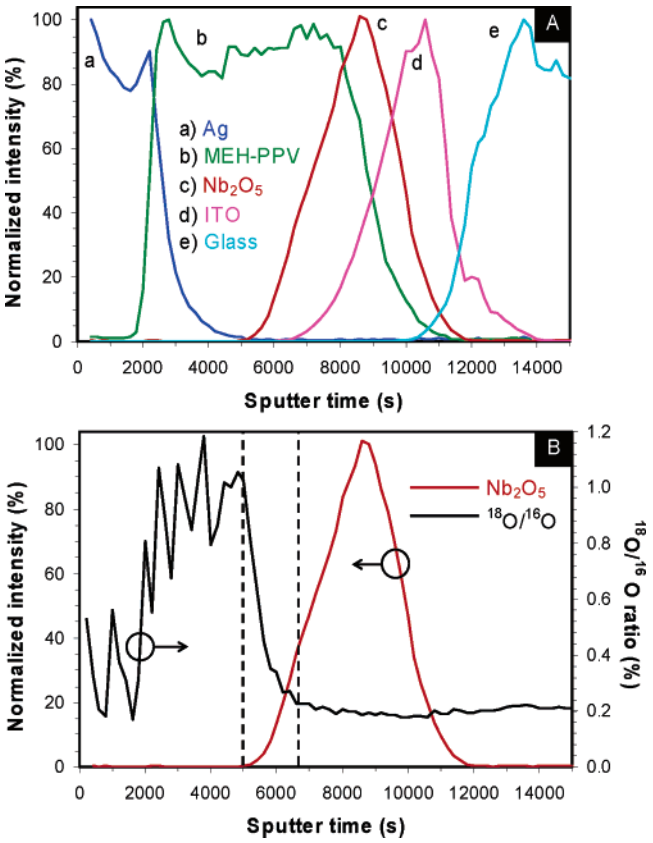

Figure 3. Depth profiles obtained by sputtering through the entire device. The experimental conditions that were necessary to sputter through the entire device contributed to a poor depth resolution. (A) The mass spectral markers used were $^{107}Ag^-$ (a), C_9^- (b), NbO_2^- (c), InO_2^- (d), and Si^- (e). (B) The vertical dashed lines represent the time window where both ^{18}O incorporation and Nb_2O_5 were detected.

MEHPPV) the HSC active area (dashed green box). Figure 4B,C is the actual TOF-SIMS images that visualize the lateral distribution of $^{18}O/^{16}O$ ratios for the illuminated device (B) and the device that was stored in darkness (C). Figure 4D displays the intensity bar used for the visualization; that is, white corresponds to the maximal ratio and black corresponds to the minimal ratio.

Figure 4E contains line profiles for the two images (B and C). The line profiles correspond to an average of all the line profiles between the two horizontal green dashed lines (part of the green box) in Figure 4B,C. The $^{18}O/^{16}O$ ratio distribution is clearly inhomogeneous for the illuminated device in particular with relatively large $^{18}O/^{16}O$ values outside what used to be the HSC active area.

If ^{18}O is indeed incorporated in Nb_2O_5 then this is the expected outcome; that is, the Ag and MEHPPV layers will impede the oxygen transport and thus slow down the incorporation. However, one could argue that the observed incorporation originates from insufficient removal of MEHPPV, which is not unrealistic considering the extremely high sensitivity of TOF-SIMS. In order to confirm our assumption that Nb_2O_5 incorporates ^{18}O, two pristine Nb_2O_5 substrates were subjected to $^{18}O_2$ atmosphere for 48 h; one was subjected to illumination, and the other was kept in the dark as a reference. The two samples were subsequently analyzed with TOF-SIMS depth profiling, and the $^{18}O/^{16}O$ ratio was thus correlated with the depth of the Nb_2O_5 layer.

(56) Norrman, K.; Krebs, F. C. *Surf. Interface Anal.* **2004**, *36*, 1542−1549.
(57) Norrman, K.; Krebs, F. C. *Sol. Energy Mater. Sol. Cells* **2006**, *90*, 213−227.

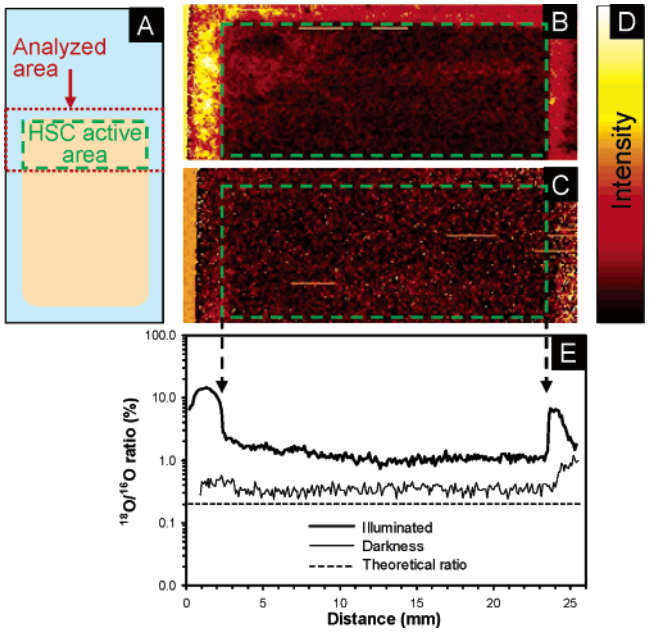

Figure 4. TOF-SIMS images of devices where the silver electrode and active layer had been removed prior to analysis. The device geometry showing the outline of the substrate and the silver electrode as an off-white shading (A). The cells were imaged over a 25 × 10 mm^2 area indicated by the dashed red square (A). The graph (E) shows line profiles of the $^{18}O/^{16}O$ distribution for the illuminated sample (B) and for the sample stored in darkness (C). The horizontal dashed black line in the graph (E) corresponds to the theoretical ratio (0.2%) for atmospheric oxygen. The profiles correspond to an average of all line profiles between the horizontal dashed green lines indicated in each image (B and C).

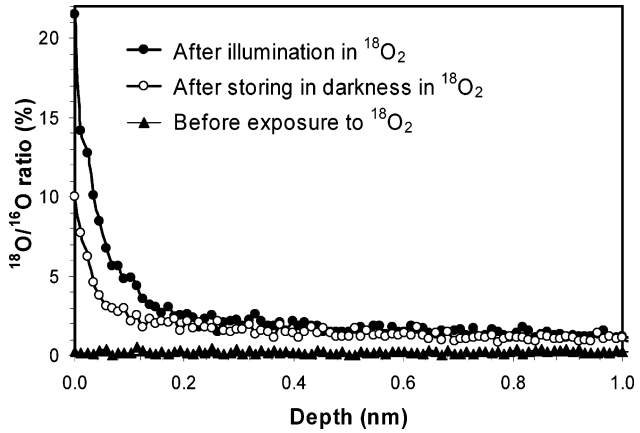

Figure 5. Depth profiles showing $^{18}O/^{16}O$ ratios as a function of sputter depth for Nb_2O_5 substrates. The sputtering rate was calibrated with respect to real space layer thickness by correlation with the density profile as determined by X-ray reflectometry.

In Figure 5 three profiles are plotted showing $^{18}O/^{16}O$ ratios as a function of depth. One shows the depth profile before exposure to $^{18}O_2$ and light (▲), one shows the profile after exposure to $^{18}O_2$ and light (●), and one shows the profile after exposure to $^{18}O_2$ but no light (○). The fact that incorporation is observed for the exposed substrates confirms that the ^{18}O incorporation in the Nb_2O_5 layer in the photovoltaic devices is real. Furthermore, the $^{18}O/^{16}O$ ratio at zero depth (i.e., the outer surface) for the Nb_2O_5 substrate that was stored in darkness is approximately half compared to the corresponding ratio for the illuminated substrate. This suggests a possible thermal contribution that is approximately equal to the contribution from the light (when illuminated for 48 h). Finally, it is evident from Figure 5 that the incorporation of ^{18}O has diminished drastically at a depth of 0.2 nm for both Nb_2O_5 substrates, which corresponds to the outer atomic oxide layer, that is, the incorporation is extremely surface specific and thus not a bulk phenomenon at the temperature produced by the sun simulator (72 °C). Both ratios are observed to be slightly higher at 0.2 nm compared to the theoretical ratio (0.2%) for atmospheric oxgyen and decrease only slightly through the remaining Nb_2O_5 layer. Possible explanations for this observation could be microscopic holes in the Nb_2O_5 layer causing ^{18}O incorporation on the inside surface of the holes as described previously for an aluminum electrode[57] or interlayer mixing caused by the sputter process. The implications of the findings described in this section are that atmospheric oxygen quickly penetrates the silver electrodes and makes its way into the layers of the solar cell all the way to the niobium oxide (within a few minutes) influencing the photovoltaic properties.[32−35]

Atmosphere−Polymer Interactions. The TOF-SIMS labeling experiment demonstrated that oxygen is incorporated into the semiconductor oxide and into the bulk of the polymer (see Figure 3) during photovoltaic operation. There are at least two possible ways to account for the oxygen incorporation in the polymer. First, polymer bleaching (oxidation) is inevitable and will account for a large part of the oxygen incorporation. Second, the possible existence of a charge-transfer complex (CTC) between the polymer and oxygen might facilitate the generation of charge carriers[58] and act as an oxygen transport pathway. Park et al.[59] have proposed the formation of $MEHPPV^{\bullet+}/O_2^{\bullet-}$ complexes formed by the photoinduced electron transfer between MEHPPV and oxygen. This CTC has been proven to improve photovoltaic response;[52,53] the CTC formation is reversible[58−60] and not linked to the formation of singlet-oxygen which is known to produce covalent oxidation products and irreversible degradation of the polymer.[61,62] If a CTC is formed it can be identified by analyses of the photoaction spectra of the solar cell and the UV−vis absorption spectra of the polymer.[7b,58,63] Thus, a shift toward the near-IR wavelength is an indication of the formation of the CTC.[55,63] A comparison between the photoaction spectra of the solar cell (Figure 6a) with the UV−vis absorption spectra of the polymer MEHPPV (Figure 6b) and the corresponding spectra for the thin film Nb_2O_5 (Figure 6c) does not present these features. First of all, the shape of the polymer spectra and that of the photoaction spectra of the HSC are similar, which suggests that the absorption in the polymer MEHPPV is mainly responsible for the photocurrent generation in the cell. Moreover, there is an absorption band at wavelengths around 350 nm (marked with an arrow) attributed to the direct band

(58) Abdou, M. S. A.; Orfino, F. P.; Son, Y.; Holdcroft, S. *J. Am. Chem. Soc.* **1997**, *119*, 4518−4524.
(59) Park, S.-J.; Gesquiere, A. J.; Yu, J.; Barbara, P. F. *J. Am. Chem. Soc.* **2004**, *126*, 4116−4117.
(60) Yu, J.; Hu, D.; Bárbara, P. F. *Science* **2000**, *289*,1327−1330
(61) Ogilby, P. R.; Kristiansen, M.; Clough, R. L. *Macromolecules* **1990**, *23*, 2698−2704.
(62) Scurlock, R.; Wang, B.; Ogilby, P. R.; Sheats, J. R.; Clough, R. L. *J. Am. Chem. Soc.* **1995**, *117*, 10194−10202.
(63) Abdou, M. S. A.; Orfino, F. P.; Xie, Z. W.; Deen, M. J.; Holdcroft, S. *Adv. Mater.* **1994**, *6*, 838−840.

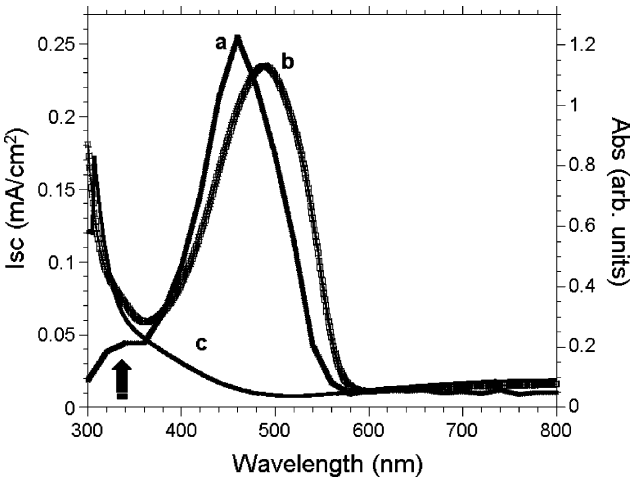

Figure 6. The action spectrum of an ITO/Nb_2O_5/MEHPPV/Ag device under the ambient atmosphere (a). For comparison purposes, the UV−vis absorption spectra for the conjugated polymer MEHPPV (b) and the Nb_2O_5 thin film (c) are shown.

gap excitation of Nb_2O_5. A comparison of the photoaction spectra with the UV−vis absorption spectra for the devices shows a slight blue shift in the maxima of the photoaction spectra which is attributed to thin film interferences. We thus rule out that a CTC contributes significantly to the oxygen incorporation.

Polymer−Oxide Interactions. We have shown that atmospheric oxygen is a prerequisite for a properly functioning HSC device based on the transparent semiconductor oxide Nb_2O_5. Furthermore, we have demonstrated that Nb_2O_5 is in equilibrium with molecular oxygen during illumination giving rise to oxygen exchange ("breathing"). Our findings reveal that the oxygen exchange is a requirement of the Nb_2O_5 electrode to maintain an optimal photovoltaic response. The release of oxygen from the semiconductor oxide could lead to irreversible degradation of the polymer at the interface and in the bulk. The possible design of a semiconductor oxide−polymer HSC device operating under inert conditions would thus have to encompass the oxygen release mechanisms of the oxide such that either oxygen is not released or such that oxygen does not react with the polymer.

Conclusions

We have studied oxygen diffusion and interaction in a working hybrid polymer solar cell based on thin films of niobium oxide and the conjugated polymer MEHPPV. The incorporation and transport of oxygen through the cell was quantified using a combination of isotopic labeling, TOF-SIMS analysis, and depth profiling. We found that oxygen is transported through the silver metal electrode and MEHPPV layer all the way to the niobium oxide film where exchange of the oxygen takes place under illumination and to a lesser extent in the dark. This oxygen breathing mechanism of the oxide was found to be linked to variations in the performance of the solar cell. When the solar cell was operating oxygen was required for good function of the device. Removal of oxygen by replacing the atmosphere by argon or vacuum led to a decrease in device performance. Reintroduction of oxygen led to immediate recovery of the solar cell function. We also observed that a stabilization period of the cell for 48 h in the dark after preparation gave the best performance and also that operation of the device in an oxygen containing atmosphere led to degradation of the device. Our results indicate that while oxygen is required for function it also leads to degradation of the solar cell.

Acknowledgment. This work was supported by the Danish Technical Research Council (STVF 2058-03-0016, STVF 26-04-0073) and the Danish Strategic Research Council (DSF 2104-04-0030, DSF 2104-05-0052). Acknowledgment is given to the Agència de Gestió d'Ajuts Universitaris i de Reserca (AGAUR, Catalunya Goverment) and to the "Ramon y Cajal" program from the Ministry of Science and Technology (Spain). We acknowledge Prof. Martin Meedom Nielsen, Risø National Laboratory, for providing the analysis software used in the reflectometry study.

CM061429D